Experimental Model Based Attitude Control Algorithms for a Quadrotor Unmanned Vehicle

Mert Önkol and Mehmet Önder Efe*

Abstract This paper focuses on modeling and control of a quadrotor type unmanned aerial vehicle (UAV). Low level control issues are addressed, the derivation of the dynamic model is presented, transient and steady state behavior of the propulsion due to motors are elaborated by the aid of artificial neural networks, and a model is developed. Several simulation works have been discussed. These include proportional integral and derivative (PID) control scheme, sliding mode control (SMC), backstepping technique and feedback linearization. A comparison of the approaches is presented in terms of the tracking precision, applicability of control signals and the qualities of the transient response.

Keywords Quadrotor, PID, feedback linearization, sliding mode control, backstepping

1 Introduction

The main motivation of UAV research is the diversity of their applications; especially the low-cost manufacturability and lightweight structure make them appealing for dangerous missions. Vertical Take-off and Landing (VTOL) vehicles are flying robots that can hover, take off and land vertically without requiring runway or landing field. The quadrotor type UAV is a typical VTOL vehicle studied several times in the past. Since the high level functions such as video transmission, object tracking and surveillance depend heavily on the low level command and control precision, this work is devoted to the low level control issues on a quadrotor type vehicle being developed at UAV Laboratory of TOBB ETU. Since the number of the control inputs is less than the number of degrees of freedom, such type of UAVs are called underactuated mechanical systems. The nonlinear, multivariable and coupled characteristics make the control of a UAV a tedious task. Several examples of trajectory tracking controllers, which are inevitably nonlinear, for quadrotors in continuous time have been investigated in the literature [1-5]. Bouabdallah

* Department of Electrical and Electronics Engineering
TOBB Economics and Technology University, Turkey
Tel: +90-312-292 4064
Fax: +90-312-292 4180
Email {monkol,onderefe}@etu.edu.tr

et al propose SMC, backstepping techniques and apply these methods successfully on a lightweight quadrotor system, [6]. Their work suggests using backstepping control technique as it is capable of controlling the orientation angles in the presence of relatively high perturbations properties. In [7], Kis et al implement backstepping control approach on a quadrotor type UAV on an embedded computer. Fang et al investigate feedback linearization and continuous time SMC for a quadrotor UAV in [8] and emphasize that continuous SMC is preferable due to the associated robustness against uncertainties and disturbances. The cited references show the state-of-the art of the UAV design concept and the associated low level as well as high level control concepts involving motor control, vision, navigation, surveillance, tracking, autonomous behavior etc.

In this paper several linear and nonlinear control schemes are used to stabilize the attitude of the vehicle developed at the UAV laboratory. The methods considered are PID, SMC, backstepping control and feedback linearization based control. The three term nature of PID scheme enables the designer to prototype the feedback control rapidly. The philosophy of the scheme is to construct a control signal based on the current value of the error, its tendency, computed via the derivative term, and its accumulated value, computed via the integral term. Several approaches to improve the performance of PID controllers are available; one approach is to utilize integrator antiwindup, [9,10]. Although the PID scheme gives a clear insight to the designer, the maximum performance with such an approach is generally limited and processes like the one here demands more sophisticated approaches leading the designer to explore the nonlinear techniques. Sliding mode control is a frequently used approach employing switching based discontinuity and displaying robustness to some extent. The philosophy of the SMC approach is to create an attractor in the phase space spanned by the error and its derivatives such that the selected subspace is stable and its attractor is at the origin. To paraphrase, once the trajectories are constrained to stay on this particular subspace, they eventually end up with the convergence to origin. It is interesting to note that this subspace, called switching hypersurface, is the boundary of a two sided decision mechanism imposing sign like terms in the control signal [11,12]. The major advantage of exploiting this scheme is its robustness against disturbances and modeling errors, which are the typical issues in the low level control of actuation mechanism of UAVs, [13]. Another method we consider in this work is backstepping method, [14,15]. The backstepping design introduces virtual variables and divides the design procedure into steps. Every step has its own Lyapunov function and the final stage of the design assumes the sum of all those Lyapunov functions and proves the negativitiy of its time derivative, [16]. Finally, we focus on feedback linearization technique, which is a standard approach in nonlinear control applications. The approach involves coming up with a transformation of the nonlinear system into a linear system via nonlinear feedback, [17-19]. Once the linear model is obtained, the remaining issue is to shape the closed loop by appropriately selecting the feedback gains.

Although the dynamic modeling of quadrotor is studied by many researchers, [20-23], the issues related to the propulsion modeling is not highlighted. To be more explicit, in simulation, the controller produces the control signals and these are applied to the inputs of the dynamic model, however, the physical system inputs are pulse width modulated

(pwm) signals. Therefore, the controller side and the model side must be separated properly. This paper focuses on such a modeling issue together with the limited power utilities available on the vehicle. This is one critical contribution of the current study.

This paper is organized as follows: The second section derives the dynamic model of the quadrotor we build and presents its physical parameters. The third section emphasizes the propulsion dynamics and its modeling by the use of artificial neural networks. This section enables to improve the dynamic model for simulation purposes, and next, we consider the PID, SMC, backstepping and feedback linearization techniques in turn. A comparison of the approaches in presented at the end of the paper.

2 Dynamic Model of the Quadrotor UAV

Derivation of dynamic model of a quadrotor type UAV is the central part of the low level control implementation. In this part, derivation of the dynamic model of the quadrotor UAV is considered. The vehicle can be represented as a four rotor body as shown in Fig. 1.

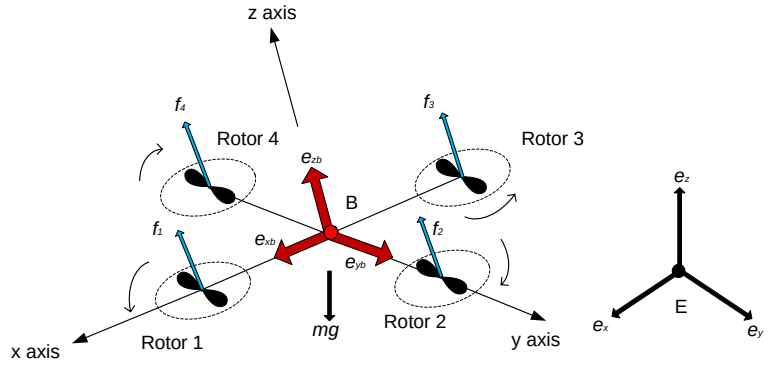

Fig. 1 Quadrotor configuration and the choice of coordinate frames

The rotor rotation directions are opposite in order to balance torque produced by rotors therefore rotor 1 and rotor 3 are rotating in the counter-clockwise direction while rotor 2 and rotor 4 rotate in the clockwise direction. Altering the angular rotor speeds causes motion in the Cartesian space. Considering the hover state, a balanced increase/decrease in the thrusts causes change in the altitude. Varying the rotor 1 and rotor 3 angular speeds inversely proportional will result a motion in x direction because of the change in pitch angle. Varying the rotor 4 and rotor 2 angular speeds inversely proportional will result a motion in y direction because of the change in roll angle. Angular speed difference of four rotors will result drag torque and yaw motion. Quadrotor UAV is modeled under the following assumptions.

- The quadrotor structure is rigid and symmetrical
- The quadrotor center of mass and body-fixed frame coincides
- Thrust and drag forces are proportional to the square of the propellers' speeds
- Ground effect is neglected
- The propellers are rigid

Suppose that E denotes earth fixed frame and B denotes body fixed frame which can be seen in Fig. 1, the airframe orientation is denoted by R matrix. R stands for the rotation from B to E. The dynamic model of quadrotor is derived from Newton-Euler approach. The dynamic equations of quadrotor can be written as follows [24].

$$\begin{bmatrix} mI_{3\times3} & 0 \\ 0 & I \end{bmatrix}\begin{bmatrix} \dot{\vec{V}} \\ \dot{\vec{\omega}} \end{bmatrix}+\begin{bmatrix} \omega\times m\vec{V} \\ \omega\times I\vec{\omega} \end{bmatrix}=\begin{bmatrix} F \\ \tau \end{bmatrix} \tag{1}$$

With the diagonal inertia matrix $I\in R^{3\times3}$, ω is the body angular velocity, $\vec{V}$ is the body linear speed vector. The dynamics in (1) can be explained as follows:

$$\dot{\zeta}=v \tag{2}$$

$$\dot{v}=-ge_z+\frac{1}{m}TRe_z \tag{3}$$

$$sk(\omega)=R^T\dot{R} \tag{4}$$

$$I\dot{\omega}=-\omega\times I\omega+\tau_a-\tau_g \tag{5}$$

where the $z = [x \quad y \quad z]^T$ denotes the position of the center of mass of the quadrotor B relative to E and describing linear motion of vehicle, v is a vector including the linear velocities of the body frame. Translational dynamics derived from Newton's second law of motion and ge_z is gravitational acceleration in z axis where $e_z=[0 \quad 0 \quad 1]^T$ denotes unit vector in earth-fixed frame in (3). T is the total thrust force generated by four rotors and m is the mass of the vehicle. The matrix R, given in (6), is an orthogonal homogeneous transformation matrix defined using Euler angles ϕ (roll), θ (pitch) and Ψ (yaw) [25]. R is used to transfer forces acting on the vehicle into earth fixed frame. The derivative of the rotational matrix to the rotational matrix by a matrix known as the Skew Symmetric Matrix in (4) where Ω represents the angular velocity of the craft relative to the body frame axis and x denotes the cross product of the two vectors. V represents any real vector. In (5) controllable inputs are available based on Newtonian relationship. Torque is equal to inertia multiplied by rotational acceleration. Torques present in the quadrotor is formulated in (5).

$$R(\phi,\theta,\psi)=\begin{bmatrix} c_\psi c_\theta & c_\psi s_\theta s_\phi - s_\psi c_\phi & c_\psi s_\theta c_\phi + s_\psi s_\phi \\ s_\psi c_\theta & s_\psi s_\theta s_\phi + c_\psi c_\phi & s_\psi s_\theta c_\phi - s_\phi c_\psi \\ -s_\theta & c_\theta s_\phi & c_\theta c_\phi \end{bmatrix} \tag{6}$$

Expression in (3) can be written as in (7), where *m* stands for the mass of the vehicle.

$$F_b = -mge_z + Re_z \sum_{i=1}^{4} T_i \tag{7}$$

In (7) F_b is the result of the forces generated by four rotors. T_i is thrust generated by each rotor. Denoting ω as the angular body rate of the airframe in body-fixed frame, angular body rate and Euler angle parameterization relationship can be given as in (8).

$$\omega = \begin{bmatrix} 1 & 0 & -s_\theta \\ 0 & c_\phi & c_\theta s_\phi \\ 0 & -s_\phi & c_\phi c_\theta \end{bmatrix} \begin{bmatrix} \dot{\phi} \\ \dot{\theta} \\ \dot{\psi} \end{bmatrix} \tag{8}$$

The quadrotor displays low amplitude angular motions letting us consider the small angle approximation for the angular body rates Small Angle Approximation (SAA) has been considered during dynamic modeling studies. Bouabdallah et al [6] find simulation test results reasonable by modeling with SAA. Hoffman et al [26] create a dynamic model based on SAA. Another utilization of SAA is presented in [27] and satisfactory results are found, i.e. $\omega = [\dot{\phi}\ \dot{\theta}\ \dot{\psi}]^{\mathrm{T}}$ and the rotational dynamics of the quadrotor are described in (5). The gyroscopic effect due to rigid body rotation is given by $-\omega \times I\omega$ which is given in (9).

$$-\omega \times I\omega = \begin{bmatrix} (I_{yy} - I_{zz})\dot{\theta}\dot{\psi} & (I_{xx} - I_{yy})\dot{\theta}\dot{\phi} & (I_{zz} - I_{xx})\dot{\phi}\dot{\psi} \end{bmatrix}^{\mathrm{T}} \tag{9}$$

τ_g is gyroscopic effect due to propeller orientation change that needs to be handled carefully, [14, 15]. τ_g is defined as:

$$\tau_g = \sum_{i=1}^{4} (\Omega \times J_r)(-1)^{i+1} \omega_i e_z \tag{10}$$

J_r is the propeller inertia, ω is propeller angular speeds. The gyroscopic effect caused by propellers only effects the dynamics of the vehicle during roll and pitch motion which can be seen from equations above. The control moments denoted by τ_a, which are produced by the actuation periphery, is given in (11).

$$\tau_a = \begin{bmatrix} \tau_{roll} & \tau_{pitch} & \tau_{yaw} \end{bmatrix}^{\mathrm{T}} = \begin{bmatrix} l(T_4 - T_2) & l(T_1 - T_3) & -Q_1 + Q_2 - Q_3 + Q_4 \end{bmatrix}^{\mathrm{T}} \tag{11}$$

With these terms, the complete dynamics of the vehicle is described in (12).

$$
\begin{aligned}
\ddot{x} &= (c_\phi s_\theta c_\psi + s_\phi s_\psi)\frac{1}{m}U_1 \\
\ddot{y} &= (c_\phi s_\theta s_\psi - s_\phi c_\psi)\frac{1}{m}U_1 \\
\ddot{z} &= -g + (c_\phi c_\theta)\frac{1}{m}U_1 \\
\ddot{\phi} &= \dot{\theta}\dot{\psi}\left[\frac{I_{yy} - I_{zz}}{I_{xx}}\right] + \frac{J_r}{I_{xx}}\dot{\theta}\Omega_d + \frac{l}{I_{xx}}U_2 \\
\ddot{\theta} &= \dot{\phi}\dot{\psi}\left[\frac{I_{zz} - I_{xx}}{I_{yy}}\right] - \frac{J_r}{I_{yy}}\dot{\phi}\Omega_d + \frac{l}{I_{yy}}U_3 \\
\ddot{\psi} &= \dot{\theta}\dot{\phi}\left[\frac{I_{xx} - I_{yy}}{I_{zz}}\right] + \frac{1}{I_{zz}}U_4
\end{aligned}
\tag{12}
$$

where m is the mass of the vehicle and the variable Ω_d seen in roll and pitch dynamics is defined as in (13). With this in mind, the control inputs U_1, U_2, U_3 and U_4 seen in (12) are defined in (14), where Ω_i is the angular speed (in radians per second) of the i-th rotor.

$$
\Omega_d = -\Omega_1 + \Omega_2 - \Omega_3 + \Omega_4 \tag{13}
$$

$$
\begin{bmatrix} U_1 \\ U_2 \\ U_3 \\ U_4 \end{bmatrix} = \begin{bmatrix} b & b & b & b \\ 0 & -b & 0 & b \\ -b & 0 & b & 0 \\ d & -d & d & -d \end{bmatrix} \begin{bmatrix} \Omega_1^2 \\ \Omega_2^2 \\ \Omega_3^2 \\ \Omega_4^2 \end{bmatrix} \tag{14}
$$

Defining $X = [\phi\ \dot{\phi}\ \theta\ \dot{\theta}\ \psi\ \dot{\psi}]^{\mathrm{T}}$ as the state of the attitude dynamics (i.e. $x_1 = \phi, x_2 = \dot{\phi}, x_3 = \theta, x_4 = \dot{\theta}, x_5 = \psi, x_6 = \dot{\psi}$), and $U = [U_1 U_2 U_3 U_4]^{\mathrm{T}}$ as the input vector, the state space representation of the dynamics can be given by $\dot{X} = f(X, U)$ where

$$f(X,U)=\begin{bmatrix} x_2 \\ p_1x_4x_6 + p_2x_4\Omega_d + p_3U_2 \\ x_4 \\ p_4x_2x_6 - p_5x_2\Omega_d + p_6U_3 \\ x_6 \\ p_7x_4x_2 + p_8U_4 \end{bmatrix} \tag{15}$$

$p_1=(I_{yy}-I_{zz})/I_{xx}$, $p_2=J_r/I_{xx}$, $p_3= l/I_{xx}$, $p_4=(I_{zz}-I_{xx})/I_{yy}$, $p_5= J_r/I_{yy}$, $p_6=l/I_{yy}$, $p_7=(I_{xx}-I_{yy})/I_{zz}$, $p_8=1/I_{zz}$.

Table 1 Physical Parameters of Quadrotor UAV

Total weight of the vehicle	m	0.800 kg
Gravitational acceleration	g	9.81 kg/m^2
Arm length of the vehicle(from c.g. to tip)	l	0.3 m
Moment of inertia along x axis	I_{xx}	15.67×10^{-3} kgm^2
Moment of inertia along y axis	I_{yy}	15.67×10^{-3} kgm^2
Moment of inertia along z axis	I_{zz}	28.34×10^{-3} kgm^2
Thrust factor	b	192.32×10^{-7} Ns^2
Drag factor	d	4.003×10^{-7} Nms^2
Propeller inertia	Jr	6.01×10^{-5} kgm^2

3 Experimental Modeling of the Propeller Transients

The dynamical model of a UAV like the one considered here could be obtained using the laws of physics and the approaches of Newtonian and/or Lagrangian dynamics. If the control inputs needed to observe a desired motion were immediately available, then it would be more straightforward to proceed to the closed loop control system design without worrying about the effects of the actuation periphery, which introduces some constraints shaping the transient and steady state behavior of the propulsion. Indeed, the real time picture is more complicated as the vehicle we develop is electrically powered and battery voltage is reducing as time passes. To cope with this difficulty one has to ask two questions and develop the corresponding blocks of the dynamic model for simulation and real time implementations:

- Given the battery voltage and the angular speed of the propeller (Ω_i), what would be the pwm value? The block answering this question is definitely a part of the controller as it computes the necessary pwm levels to be applied to the electronic speed controllers (See Stage 2 of Fig. 2)

- Given the battery voltage and the pwm level, what would be the angular speed of the propeller? Clearly the block answering this question is a part of the dynamic model and it is needed during the simulation work (See Stage 3 of Fig. 2).

The reason why we would like to step down from U_is to the pwm level and step up from pwm level to U_is is the fact that brushless DC motors are driven at the pwm level and we have to separate the dynamic model of the quadrotor UAV and the controller by drawing a line exactly at the point of signal exchange occurring at pwm level. Use of neural networks facilitates this in the presence of voltage loss in the batteries.

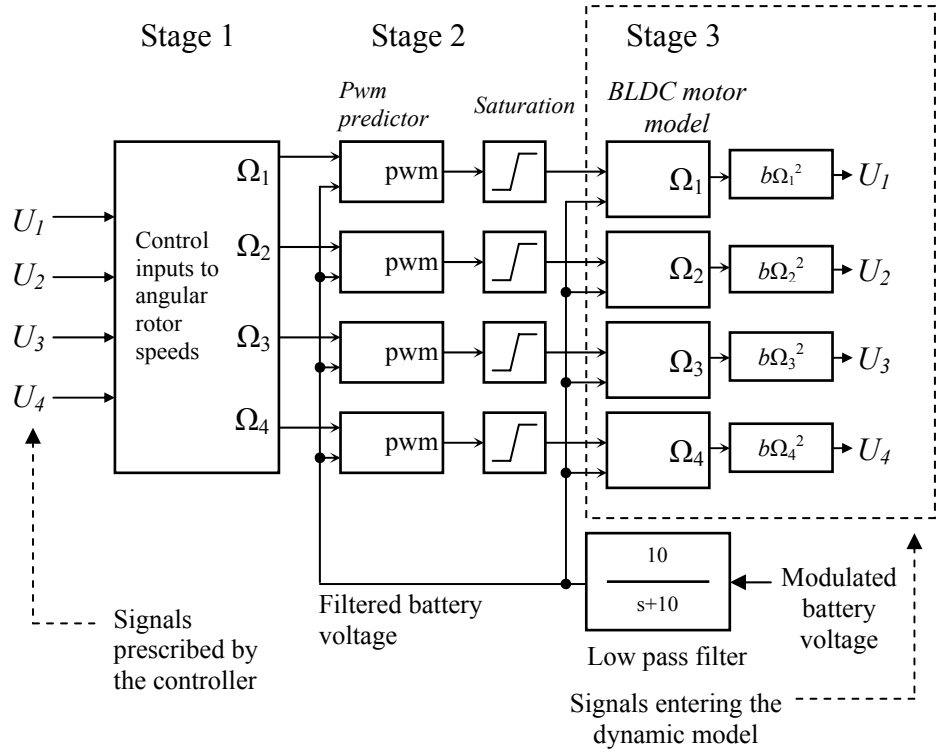

Fig. 2 Conversion of control signals $U_1,\ldots,U_4$ to those entering the dynamic model of the vehicle

In Figs. 3-4, the neural models for establishing the handshaking between the controller and the dynamic model are depicted. Clearly, proper functioning of these models entails the knowledge of b and d, the thrust coefficient and the drag coefficient, respectively. In Fig. 5(a), a six level stepwise pwm signal is shown. The signal sweeps the allowable range and endures sufficiently to observe the steady response is obtained, which are shown in Fig. 5(b). Thirty five consecutive experiments have been carried out with the

same Lithium Polymer battery and the simultaneous time traces have been recorded for post processing.

Obviously, as the experiment with the pwm profile in Fig. 4(a) is repeated, the angular speed of the rotor reduces so does the corresponding lift forces and a family of curves is obtained. Fig. 5(c) shows that the steady values of the lift forces for every distinct level of the pwm signal decreases as the experiments are repeated. Finally, the instant voltage read from the multimeter is recorded and depicted in Fig. 5(d). Clearly, the powering issues are critical in planning the mission and related navigation tasks for UAVs like the one we consider here. This picture is a good indication of extending the dynamic model and the feedback controller to where the effect of the decreasing battery voltage is addressed appropriately.

It is now clear why the use of an interface like artificial neural networks is beneficial but the filters seen in Figs. 3-4 need clarification. If a step change occurs in the pwm signal as shown in Fig. 5(a), the propulsion is observed as shown in Fig. 5(b), every step of which is more like the response of a first order system. The neural network receives the output of a first order filter $4/(s+4)$ as an auxiliary input to realize the transient correctly. After the simultaneous time traces are obtained, we utilize the Levenberg-Marquardt optimization technique to accomplish the training of the neural network. Coming to the other filter, one has to notice that the measured battery voltage is modulated severely as shown in Fig. 6(a) and in order to infer a good average value, the filtering of it is unavoidable. In Fig. 6(b), the pwm signal is shown for this experiment. After many experiments, we choose the filter $10/(s+10)$, which yields the best results. In the experiments, we discretize the filter with Tustin approach and implement it on the DSP hardware.

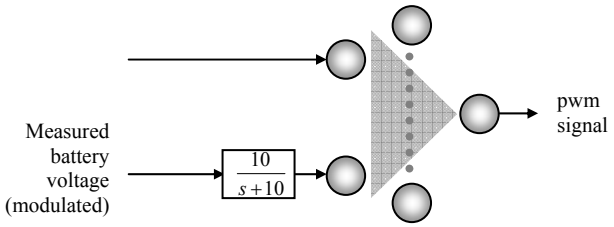

Fig. 3 Neural network component of the controller, stage 2 in Fig. 2.

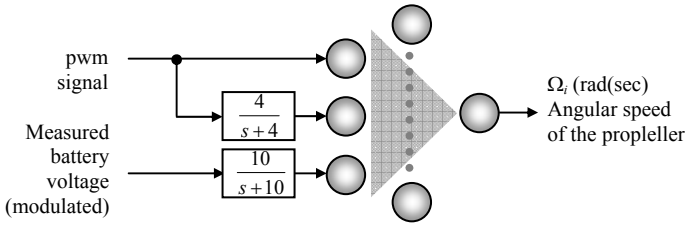

Fig. 4 Neural network component of the dynamic model, stage 3 in Fig. 2.

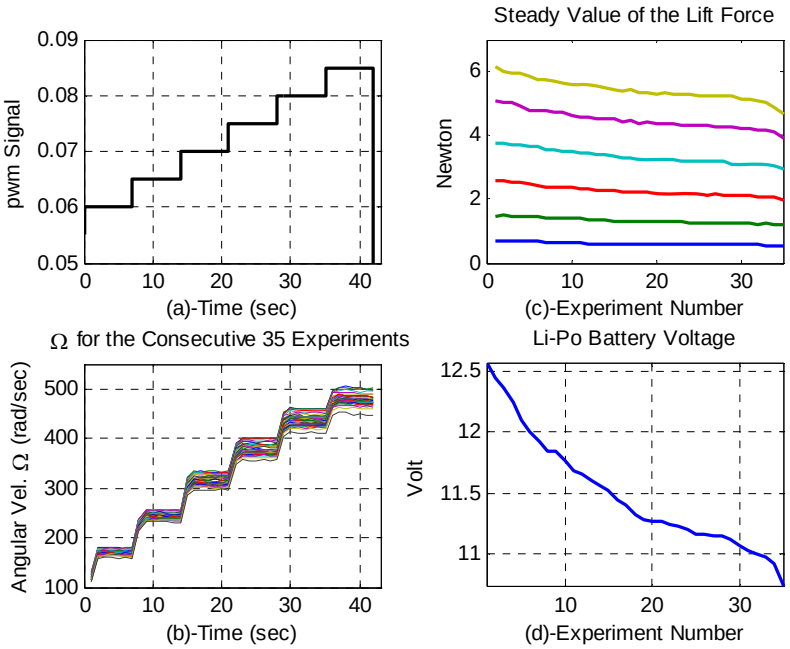

Fig. 5 The effect of the decrease in the battery voltage on the steady value of the lift force. The propeller has dimensions 12×4.5.

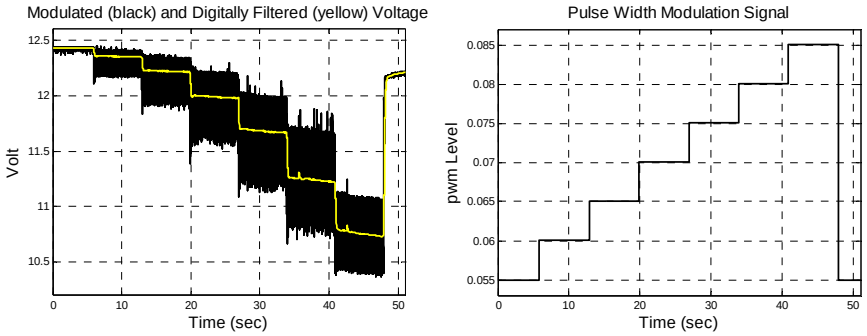

Fig. 6 (a) The modulated battery voltage and the filtered value of it. (b) pwm signal for this experiment.

The test bed includes a torque meter which is essentially a strain gauge, measuring the drag force generated by the propeller to derive the drag coefficient, *d*. The mechanism is

placed on a scale and RPM sensor is mounted appropriately to obtain the thrust generated by the propeller at distinct pwm levels letting us compute the thrust coefficient, *b*. The experimental results to determine these coefficients are summarized in Table 2. The methodology to find out the relationship between voltage difference and torque is given as follows: When the electronic speed controller receives a particular pwm signal, the motor is actuated and a thrust in the downwards direction is created, and this leads to an increment in the display of the scale as the angular speed of the rotor increases. By the use of a torque meter whose output is associated with a difference amplifier lets us obtain torque produced by propeller. The test bed is illustrated in Fig 7.

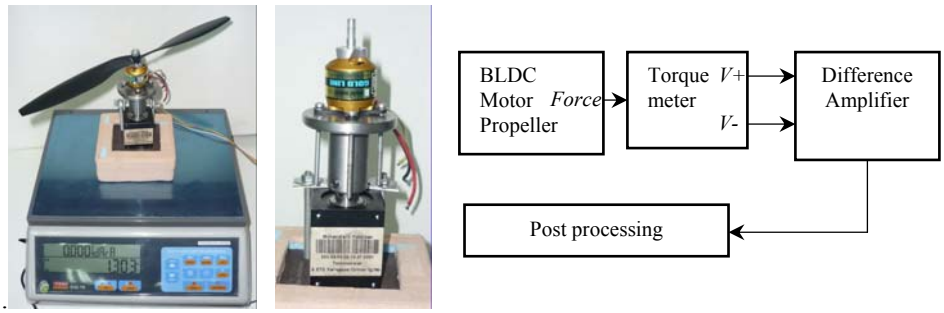

Fig. 7 (a)The experimental setup to collect data for *b* and *d* computation (b) block diagram for setup

Table 2 The experimental results leading to the average values b=192.32×10^{-7} and d=4.003×10^{-7}

pwm Signal	pwm Percentage	Torque (Nm)	Thrust (N)	Propeller speed (rad/sec)	Thrust Coefficient (b)	Drag Coefficient (d)
0.060	20%	0.013259	0.57879	169	202.65×10^{-7}	4.639×10^{-7}
0.062	24%	0.018835	0.87309	206	205.70×10^{-7}	4.432×10^{-7}
0.064	28%	0.024411	1.09872	232	204.10×10^{-7}	4.532×10-^{7}
0.068	36%	0.035563	1.64808	285	202.80×10^{-7}	4.378×10^{-7}
0.070	40%	0.041139	1.98162	324	190.78×10^{-7}	3.911×10^{-7}
0.072	44%	0.046715	2.29554	350	190.56×10^{-7}	3.834×10^{-7}
0.074	48%	0.052291	2.61927	374	187.6×10^{-7}	3.738×10^{-7}
0.076	52%	0.056473	2.92338	401	181.8×10^{-7}	3.507×10^{-7}
0.078	56%	0.063443	3.22749	425	178.68×10^{-7}	3.512×10^{-7}
0.080	60%	0.069019	3.39426	420	192.41×10^{-7}	3.912×10^{-7}
0.082	64%	0.073201	3.65913	435	193.32×10^{-7}	3.863×10^{-7}
0.085	70%	0.080171	3.98286	460	188.22×10^{-7}	3.788×10^{-7}

With average b=192.32×10^{-7} and average d=4.003×10^{-7} the neural structure shown in Fig. 4 is set by selecting a linear output neuron, single hidden layer with hyperbolic tangent type neuronal activation functions. A total of 10 hidden neurons are utilized and a pwm

profile that has not been used during the training is presented to the neural network. The results are shown in Fig. 8, where a chirp signal is used as the pwm signal and the associated prediction procedure is executed. Clearly the neural model predicts the real time measurements of the angular speed and functions as an integral part of the dynamic model of the quadrotor UAV. Although not given here due to the space limit, the neural model predicting the pwm level (See Fig. 3) is trained and incorporated into the simulation model.

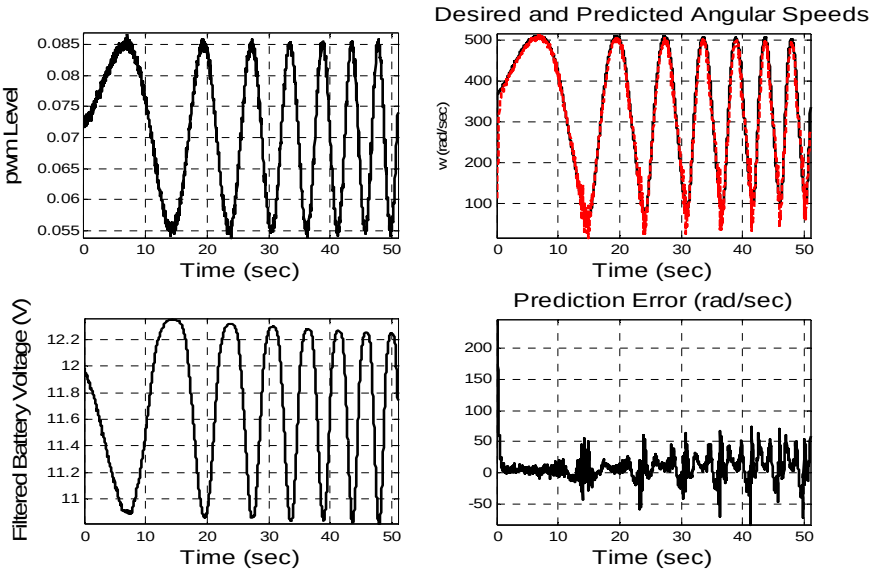

Fig. 8 The results for the neural model predicting the angular speed in the presence of battery voltage changes.

The discussion presented so far aimed at building the realistic dynamic model of a quadrotor UAV that properly handles the changes in the battery voltage. In what follows, we present the nonlinear control simulations utilizing these handshaking tools of dynamic models.

4 Attitude Control via PID Control Technique

The purpose of the PID controller is to force the Euler angles to follow desired trajectories. We consider the hover condition and set $U_1=mg$. The objective in PID controller design is to adjust the gains to arrive at an acceptable degree of tracking performance in Euler angles. The PID controller for the ϕ dynamics can be given as

$$U_2 = K_{p\phi}(\phi_d - \phi) + K_{i\phi}\int(\phi_d - \phi)\mathrm{d}t + K_{d\phi}\dot{\phi} \tag{16}$$

which implements the derivative kick to avoid adverse effects of the possible sudden changes in the command signal. More explicitly, when a step change in ϕ_r occurs, the derivative term in the conventional sense would produce a very large value and this would result in undesired spikes in the control signal. To remedy this problem, the derivative operator is applied solely to the output of the process instead of error signal, which is given in (16). In order to design the PID controllers, nonlinear rotational dynamics of quadrotor are linearized around zero, which are given by (17).

$$\phi(s) = \frac{1}{s^2}\frac{l}{I_{xx}}U_2(s) \quad \theta(s) = \frac{1}{s^2}\frac{l}{I_{yy}}U_3(s) \quad \psi(s) = \frac{1}{s^2}\frac{1}{I_{zz}}U_4(s) \tag{17}$$

The coefficients chosen are $K_{p\phi}$=2.14, $K_{i\phi}$=0.13, $K_{d\phi}$=0.66. For the pitch dynamics, we set the same values and for the yaw dynamics, $K_{p\Psi}$=0.02, $K_{i\Psi}$=0.01, $K_{d\Psi}$=0.01 are selected. Angular measurement noise with 1e−5 rad variance is added to make the simulations more realistic.

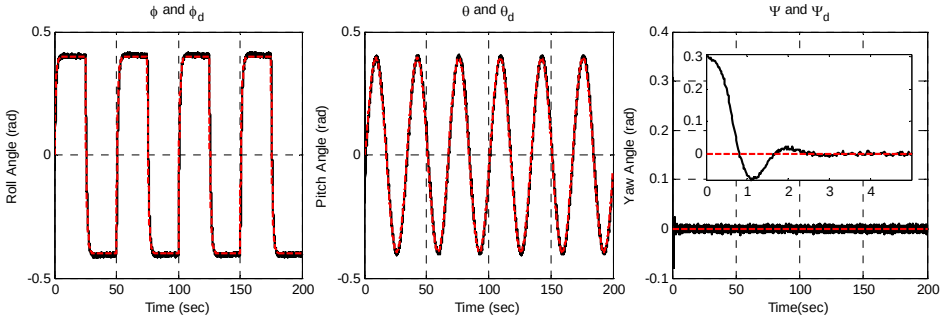

Fig. 9 The tracking results for the selected PID controllers.

The results of PID scheme are shown in Figs. 9-10, where it is seen that the attitude stabilization is obtained with satisfactory precision. Initial errors are compensated fairly quickly and the controller produces fairly smooth control signals having reasonable magnitudes. The controller tries to maintain the desired attitude by producing smooth control signals, whose initial behaviors are shown in the top row of Fig. 10, and as an example, the behavior around t=50 sec. are depicted in the bottom row of the same figure, all indicating acceptable time trends.

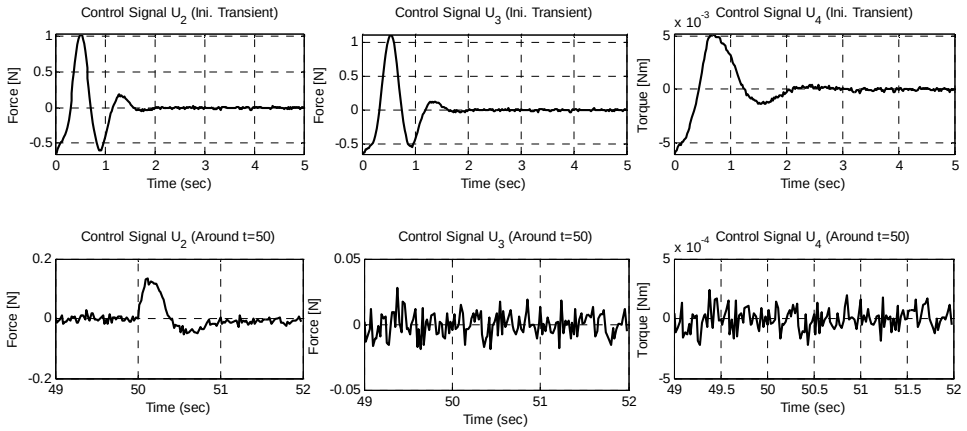

Fig. 10 The control signals for the PID control scheme U_1=7.8448 Newtons.

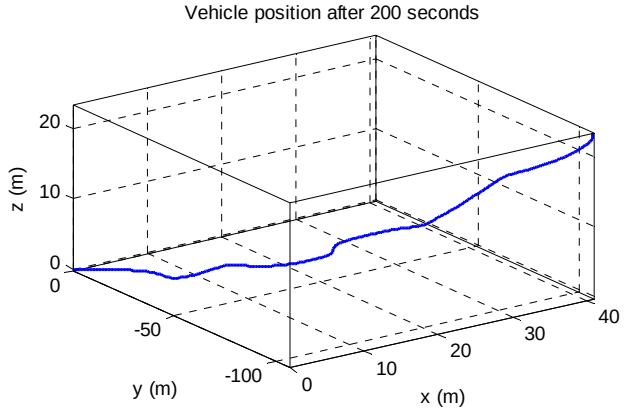

Fig. 11 Behavior in the Cartesian space.

5 Attitude Control via Sliding Mode Control Technique

Sliding mode control is a well-established nonlinear control technique that displays certain degree of robustness against uncertainties and disturbances. Although it is vulnerable to noise and it suffers from chattering phenomenon, several approaches have been proposed to overcome these difficulties without giving concessions from the robustness property of the scheme. The behavior is composed of two phases, first the error dynamics is guided toward a predefined subspace of the state space, which we call the

sliding manifold, and the behavior during this phase is called the reaching phase. This phase is known for the high magnitude control efforts that may undergo saturation sometimes. Second is the sliding phase, during which the error vector obeys the dynamical implications of the analytic description of the locus itself, which is stable by design and the error terminates at the origin inevitably. The control scheme takes its name from the latter dynamic behavior and is called sliding mode control.

Let $e_\phi=\phi-\phi_d$ be the error in roll dynamics. Sliding manifold for the roll dynamics can be written as $s_\phi = \dot{e}_\phi + \lambda_\phi e_\phi$. When $s_\phi = 0$ is reached at time t_0, the solution for t_0 is obtained as $s_\phi(t) = s_\phi(t_0)\exp(-\lambda_\phi(t-t_0))$. Now consider the Lyapunov function candidate in (18).

$$V(s_\phi) = s_\phi^2 / 2 \tag{18}$$

If the time derivative of the Lyapunov function candidate in (18) satisfies $s_\phi \dot{s}_\phi < -k_\phi |s_\phi|$ with $k_\phi > 0$, then all initial conditions of the roll error is guided toward the loci characterized by $s_\phi=0$. To maintain $s_\phi \dot{s}_\phi < -k_\phi |s_\phi|$ the control signal is chosen as follows to drive the roll angle to desired trajectory.

$$U_2 = \frac{1}{p_3}\left(-p_1 x_4 x_6 - p_2 x_4 \Omega_d + \ddot{x}_{1d} - \lambda_\phi(x_2 - \dot{x}_{1d}) - k_\phi sign(s_\phi) - k_1 s_\phi\right) \tag{19}$$

where $\dot{x}_{1d}$ denotes desired angular roll rates, $\ddot{x}_{1d}$ denotes desired angular roll acceleration. In order to avoid chattering, during the implementation stage the sign function is approximated as $sign(x) \cong x/(|x|+\varepsilon)$ with a parameter ε determining the sharpness around s=0. Next we design U_3 and U_4 by following a similar design procedure yielding

$$U_3 = \frac{1}{p_6}\left(-p_4 x_2 x_6 + p_5 x_2 \Omega_d + \ddot{x}_{3d} - \lambda_\theta(x_4 - \dot{x}_{3d}) - k_\theta sign(s_\theta) - k_2 s_\theta\right) \tag{20}$$

$$U_4 = \frac{1}{p_8}\left(-p_7 x_2 x_4 + \ddot{x}_{5d} - \lambda_\psi(x_6 - \dot{x}_{5d}) - k_\psi sign(s_\psi) - k_3 s_\psi\right) \tag{21}$$

Based on the aforementioned discussion, it is straightforward to see that λ_θ, k_θ, k_2 ,λ_ψ, k_ψ, k_3 are positive valued design parameters. In Table 3, the parameters of the SMC scheme and those of the simulations are given. In choosing the parameters determining the response of the vehicle, the real system's behavior is considered in order to avoid claiming impossible maneuvers.

The results of the simulations of SMC scheme are illustrated in Figs. 12-15. Although a similar tracking performance is observed with PID scheme, the switching nature of the control law enforces the motion to take place in the vicinity of the sliding manifold. This

is reflected naturally to phase space behavior and the control signals shown in Figs. 13 and 14, respectively. Clearly the ranges of the control signals are acceptable as well as the local fluctuations required to maintain the desired motion. The initial errors are quickly attracted by the sliding manifold, as seen in Fig. 13, and once got trapped, the errors stay there forever. The figure also provides the associated time values of the extreme points in the graphs. These time values are also adequate for a real time application of a sliding mode controller on a vehicle like the one we study here.

Table 3 Simulation Parameters for the Sliding Mode Control Scheme

Simulation Time	T	200 sec
Simulation Step Size	Δt	0.02 sec
Slope parameters	λ_φ, λ_θ, λ_Ψ	1.00
Angular measurement noise variance	$\Delta\phi$, $\Delta\theta$, $\Delta\psi$	$1e{-}5$ rad
Reaching law parameter	k_ϕ, k_θ, k_ψ	0.20
Reaching law parameter	k_1, k_2, k_3	0.10
Sign function smoothing parameter	ε	0.10
Initial values of Euler angles	$\phi(t_0), \theta(t_0), \psi(t_0)$	0.3 rad

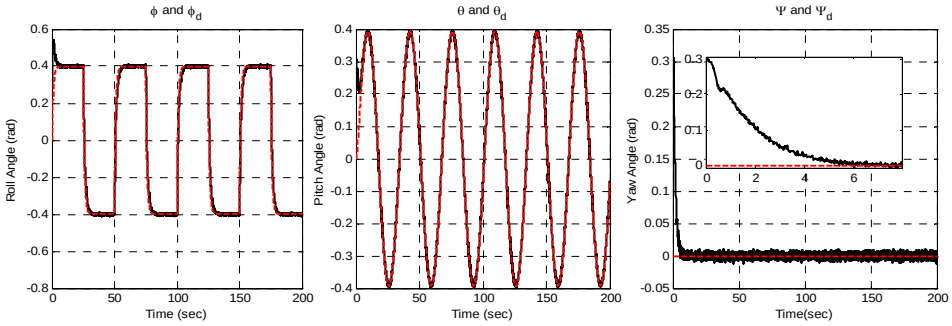

Fig. 12 The tracking results for the SMC scheme.

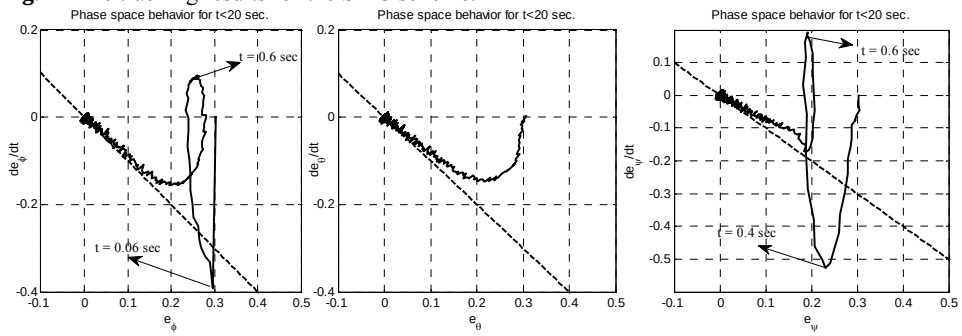

Fig. 13 Phase space behaviors of roll, pitch and yaw angles.

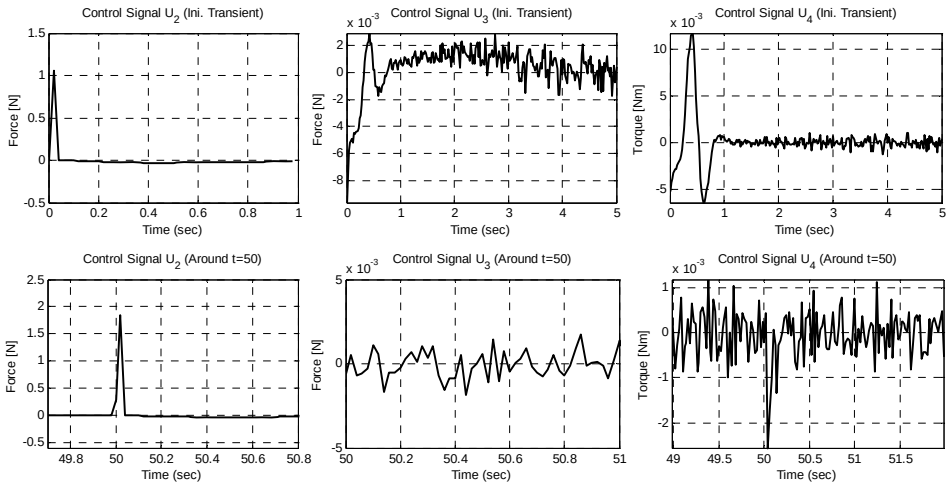

Fig. 14 The control signals for the SMC scheme U_1=7.8448 Newtons.

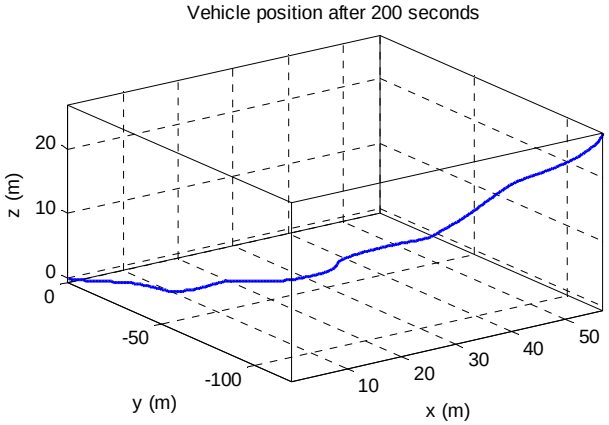

Fig. 15 Behavior in the Cartesian space.

A natural question here would focus on the robustness of the closed loop control system. In order to justify the robustness of SMC scheme, we design the controller for m=800 grams and repeat our tests for m=750 grams. The results are illustrated in Figs. 16-19 demonstrating virtually the same performance seen in Figs. 12-15.

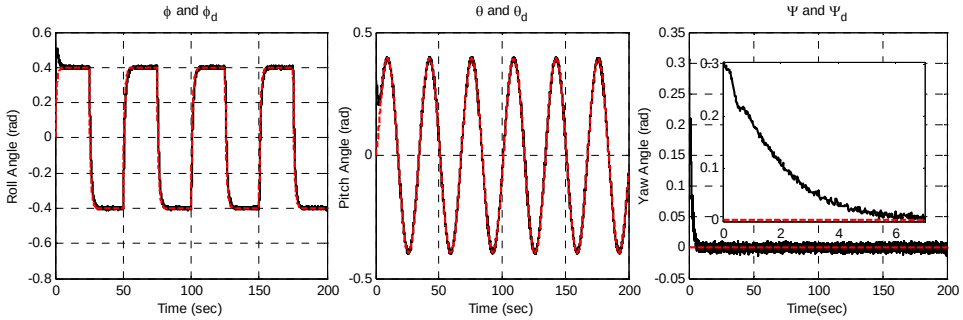

Fig. 16 The tracking results with sliding mode control scheme.

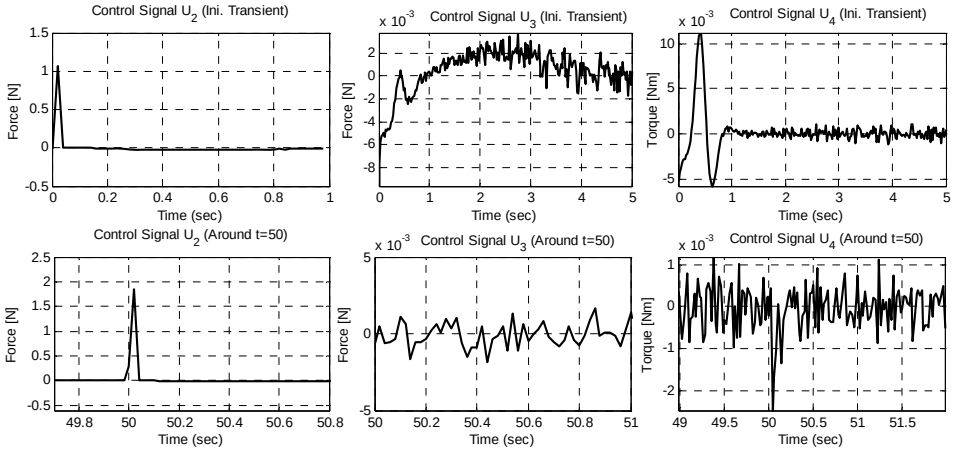

Fig. 17 The control signals for the SMC scheme U_1=7.8448 Newtons.

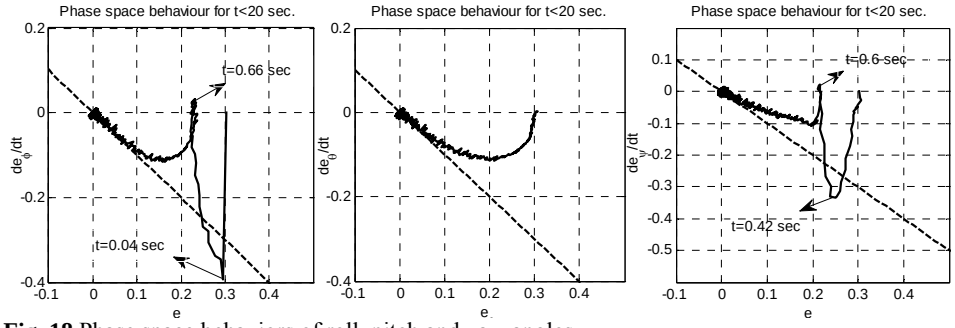

Fig. 18 Phase space behaviors of roll, pitch and yaw angles.

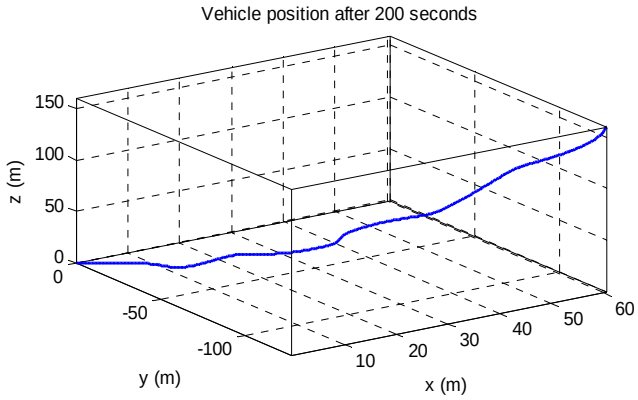

Fig. 19 Behavior in the Cartesian space.

5 Attitude Control via Backstepping Control Technique

Backstepping control scheme is based on the implementation of a control law designed via introducing virtual states and nested development of the stages. The dynamics of the quadrotor system considered in this paper is suitable for backstepping controller design and the details follow. Define first virtual state and derivative of the virtual state as, $z_1 = x_1 - x_{1d}$ and $z_2 = x_2 - \alpha_1 - \dot{x}_{1d}$, respectively. Choosing $V_1 = z_1^2 / 2$ as the Lyapunov function candidate for the first stage, the time derivative of V_1 is obtained as $\dot{V}_1 = z_1 (z_2 + \alpha_1)$. If $\alpha_1 \coloneqq -k_1 z_1$ is selected, then we have $\dot{V}_1 = -k_1 z_1^2 + z_1 z_2$. For the second stage, we choose the Lyapunov function candidate $V_2 = V_1 + z_2^2 / 2$. Since

$$\dot{z}_2 = p_1 x_4 x_6 + p_2 x_4 \Omega_d + p_3 U_2 - (-k_1 \dot{z}_1) - \ddot{x}_{1d} \tag{22}$$

The time derivative of V_2 can be written as below.

$$\begin{aligned} \dot{V}_2 &= \dot{V}_1 + z_2 \dot{z}_2 \\ &= -k_1 z_1^2 + z_2 \left(p_1 x_4 x_6 + p_2 x_4 \Omega_d + p_3 U_2 - (-k_1 \dot{z}_1) - \ddot{x}_{1d} \right) \end{aligned} \tag{23}$$

With k_2>0, if we choose the control law as given in (24), then the time derivative of the V_2 can be written as in (25).

$$U_2 = \frac{1}{p_3} (-z_1 - p_1 x_4 x_6 - p_2 x_4 \Omega_d - k_1 (z_2 - k_1 z_1) + \ddot{x}_{1d} - k_2 z_2) \tag{24}$$

$$\dot{V}_2 = -k_1 z_1^2 - k_2 z_2^2 \tag{25}$$

Repeating the same procedure for the pitch and yaw dynamics, one obtains and U_3 and U_4 as follows.

$$U_3 = \frac{1}{p_6}(-z_3 - p_4 x_2 x_6 + p_5 x_2 \Omega_d - k_3(z_4 - k_3 z_3) + \ddot{x}_{3d} - k_4 z_4) \tag{26}$$

$$U_4 = \frac{1}{p_8}(-z_5 - p_7 x_2 x_4 - k_5(z_6 - k_5 z_5) - k_6 z_6) \tag{27}$$

A number of simulation studies are carried out in Matlab/Simulink® to find the most convenient parameters to drive states of quadrotor to their desired values. Noisy observations are considered to see the disturbance rejection capability of the closed loop control system.

Table 4 Simulation Parameters for the Backstepping Scheme

Simulation Time	T	200 sec
Simulation Step Size	Δt	0.02 sec
Angular measurement noise variance	$\Delta\phi, \Delta\theta, \Delta\psi$	$1e{-}5$ rad
Design parameter	k_1, k_3, k_5	1.00
Design parameter	k_2, k_4, k_6	0.50
Initial values of Euler angles	$\phi(t_0), \theta(t_0), \psi(t_0)$	0.3 rad

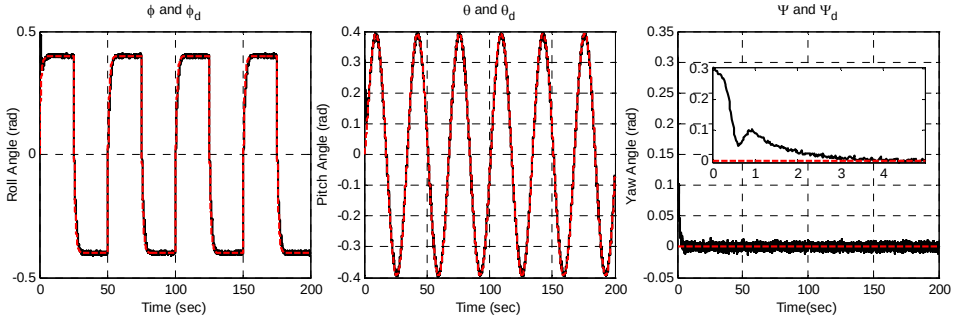

Fig. 20 The tracking results for the backstepping control technique.

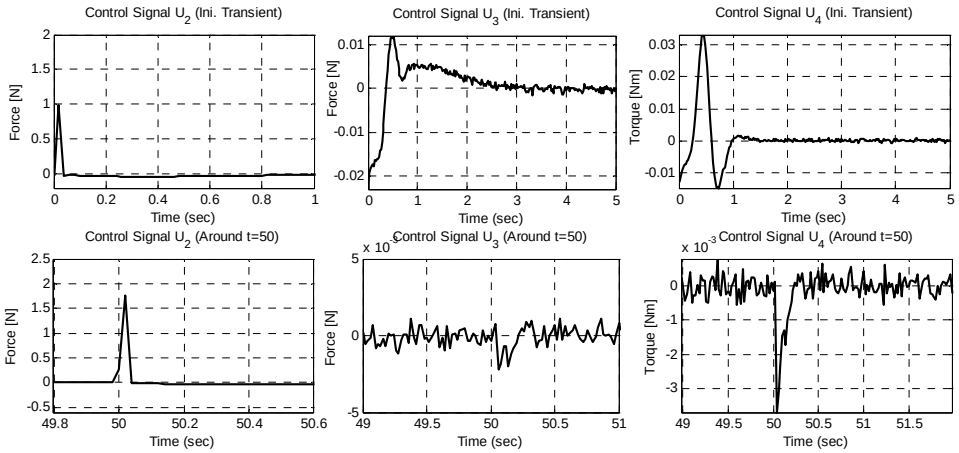

Fig. 21 The control signals for the backstepping scheme U_1=7.8448 Newtons.

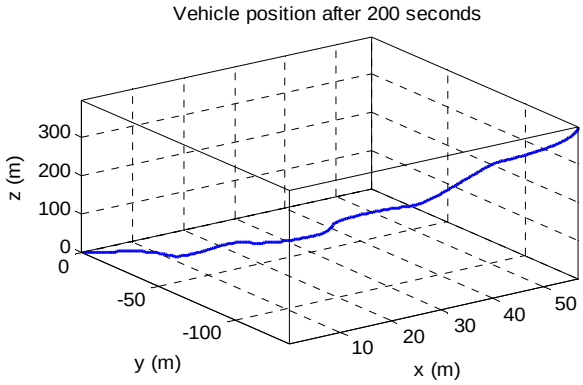

Fig. 22 Behavior in the Cartesian space.

In Figs. 20-22, the tracking performances, the control signals and the journey of the vehicle in 3D space are shown respectively. The precise tracking is one prominent feature that is seen at the first glance and the instant spikes in the control signals is the price paid for this. Backstepping technique is seen to be one alternative in real time applications of the vehicle. Robustness of the backstepping technique is tested by considering uncertainty in the mass of the vehicle, 800 grams considered for the design of the controller whereas the quadrotor had a mass equal to 750 grams. The results are seen in Figs. 23-25, which are almost indistinguishable from those seen in Figs. 20-22.

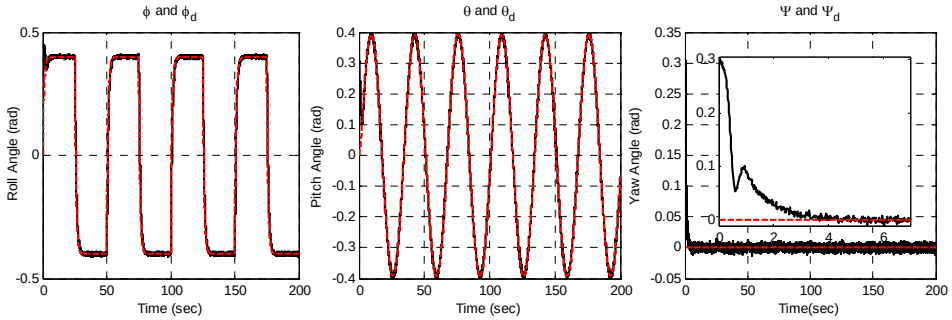

Fig. 23 The tracking results for the backstepping control technique.

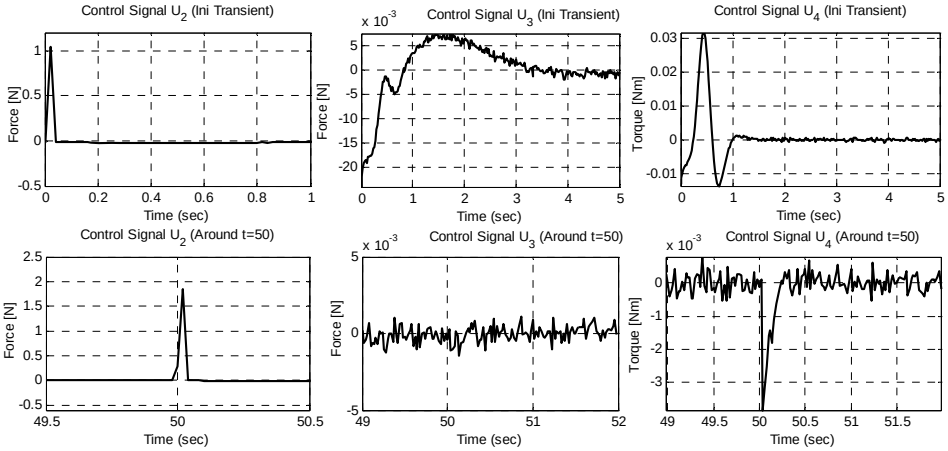

Fig. 24 The control signals for the backstepping scheme U_1=7.8448 Newtons.

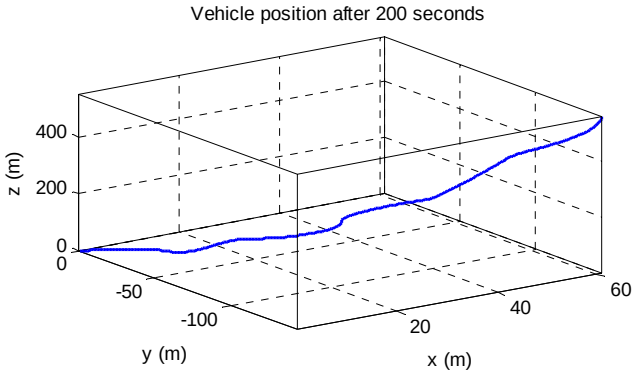

Fig. 25 Behavior in the Cartesian space

6 Attitude Control via Feedback Linearization Technique

The central idea of feedback linearization is to algebraically transform a given nonlinear system dynamics to dynamics of a linear one, so that the well established linear control techniques can be applied. Feedback linearization is achieved by exact state transformation and feedback, rather than by linear approximation of the dynamics. The relative degree and order of the roll, pitch and yaw subsystem is the same. Input-state feedback linearization can be applied to three subsystems. The nonlinear system is transformed into controllable canonical form after feedback linearization. The closed loop system is reduced to three double integrators after applying inputs U_2, U_3 and U_4. The control inputs are given in (28)-(30).

$$U_2 = \frac{1}{p_3}(-p_1 x_4 x_6 - p_2 x_4 \Omega_r + v_1) \tag{28}$$

$$U_3 = \frac{1}{p_6}(-p_4 x_2 x_6 + p_5 x_2 \Omega_r + v_2) \tag{29}$$

$$U_4 = \frac{1}{p_6}(-p_5 x_2 x_6 + v_3) \tag{30}$$

Three double integrators are $\ddot{\phi} = v_1$, $\ddot{\theta} = v_2$, $\ddot{\psi} = v_3$. The signals denoted by v_is are selected as given in (31)-(33)

$$v_1 = \ddot{\phi}_d + \lambda_1 \dot{e}_\phi + \lambda_2 e_\phi \tag{31}$$

$$v_2 = \ddot{\theta}_d + \lambda_3 \dot{e}_\theta + \lambda_4 e_\theta \tag{32}$$

$$v_3 = \ddot{\psi}_d + \lambda_5 \dot{e}_\psi + \lambda_6 e_\psi \tag{33}$$

Error signals are defined as $e_\phi = \phi_d - \phi$, $e_\theta = \theta_d - \theta$, $e_\psi = \psi_d - \psi$ and with these choices, the tracking errors are governed by the following differential equations.

$$\ddot{e}_\phi + \lambda_1 \dot{e}_\phi + \lambda_2 e_\phi = 0 \tag{34}$$

$$\ddot{e}_\theta + \lambda_3 \dot{e}_\theta + \lambda_4 e_\theta = 0 \tag{35}$$

$$\ddot{e}_\psi + \lambda_5 \dot{e}_\psi + \lambda_6 e_\psi = 0 \tag{36}$$

λ values are chosen to assign eigenvalues of linearized subsystems. Design criterion for all three subsystems is to observe critically damped response ($\xi = 1$) to step input and this requires $\lambda_1 = 2\sqrt{\lambda_2}$ $\lambda_3 = 2\sqrt{\lambda_4}$ $\lambda_5 = 2\sqrt{\lambda_6}$. The simulation settings and parameter values are tabulated in Table 5 and the results are shown in Figs. 26-28 with exact knowledge of the vehicle mass. In Figs. 29-31, we demonstrate the response of the closed loop system if there is uncertainty in the mass of the vehicle. The design phase assumes m=800 grams whereas the vehicle has m=750 grams in reality. Clearly, the results for both cases are almost indistinguishable, the initial errors are quickly driven toward zero and desired attitude is followed under the presence of measurement noise.

Table 5 Simulation Parameters for the Feedback Linearization Scheme

Simulation Time	T	200 sec
Simulation Step Size	Δt	0.02 sec
Angular measurement noise variance	$\Delta\phi, \Delta\theta, \Delta\psi$	1e–5 rad
Design parameter	λ_1	2
Design parameter	λ_2	1
Initial values of Euler angles	$\phi(t_0), \theta(t_0), \psi(t_0)$	0.3 rad

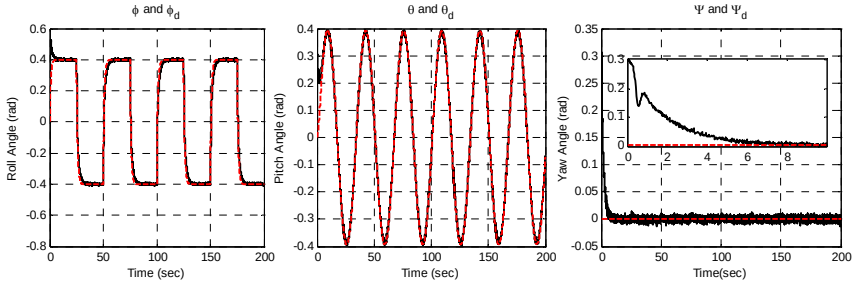

Fig. 26 The tracking results for the feedback linearization technique.

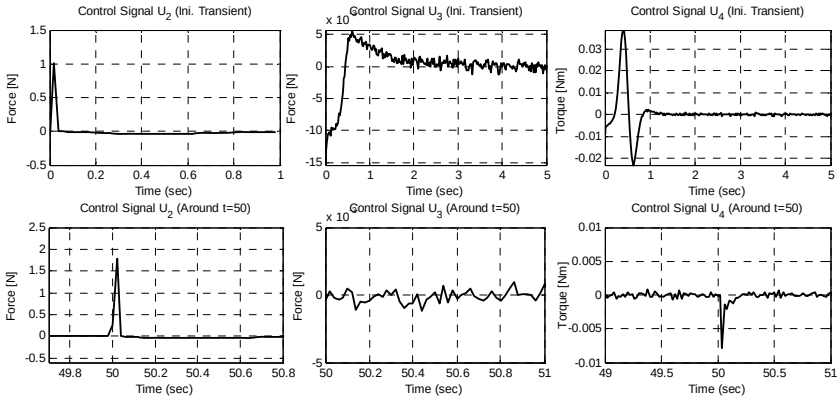

Fig. 27 The control signals for the feedback linearization scheme U_1=7.8448 Newtons.

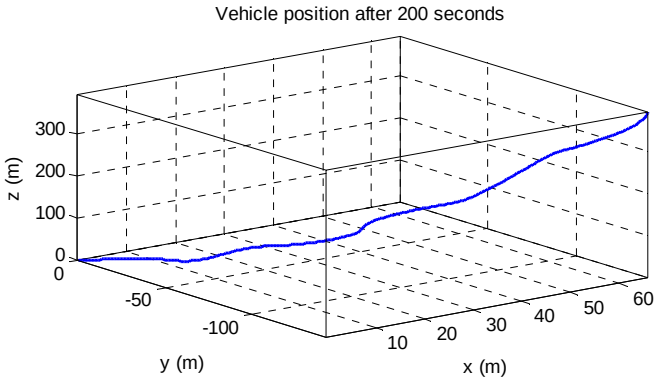

Fig. 28 Vehicle behavior in the Cartesian space.

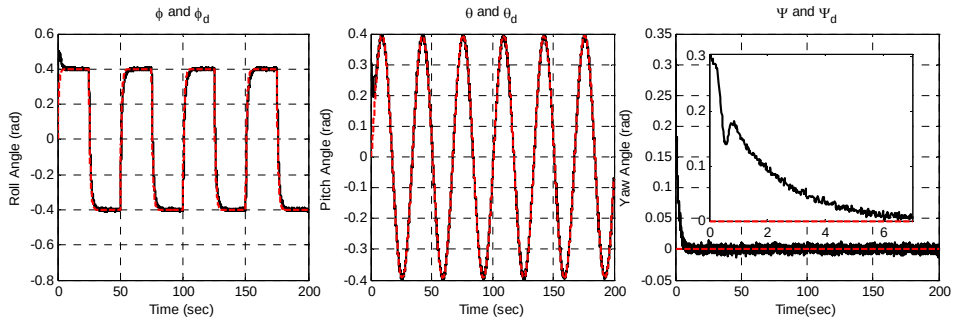

Fig. 29 The tracking results for the feedback linearization technique.

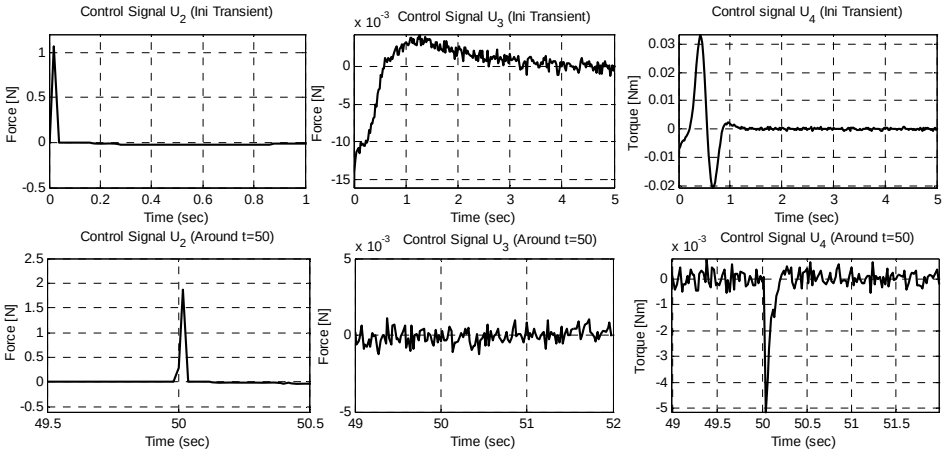

Fig. 30 The applied control signals with feedback linearization approach.

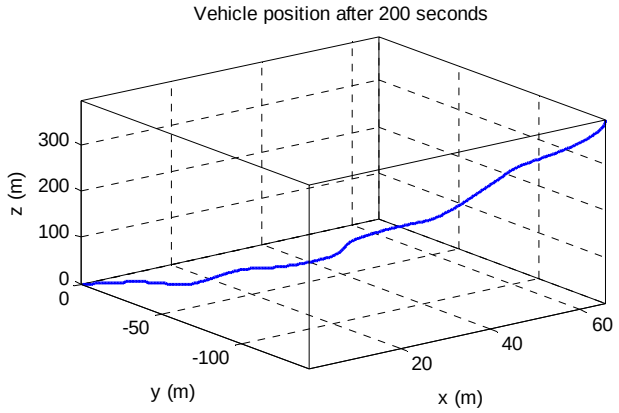

Fig. 31 Behavior in the Cartesian space

8 An Overall Assessment of the Considered Schemes

Four approaches have been simulated on a model developed through Euler Lagrange formalism and several experiments to incorporate the effect of the change in the battery voltage. Although it is optional to use such modules in simulations, yet the results of works disregarding these effects are likely to be unrealistic. PID control scheme is first implemented, SMC and backstepping designs are tested and feedback linearization scheme is implemented as the last approach. Although PID is a simple method to follow, it –even in the experiments we carry out in real time- suffers from severe disturbances available in the operation of the prototype model. Based on the simulation results, its performance is acceptable. The advantage of PID scheme is the fact that it does not require a detailed dynamic model, whereas the other methods we consider do. In spite of this picture, nonlinear control schemes are more versatile than their linear counterparts if the plant under investigation is nonlinear and performance expectations are tight. The results we obtain demonstrate that SMC scheme is able to create the sliding subspace on which the phase space motion takes place. Backstepping design and feedback linearization techniques are also based on Lyapunov stability to meet the accurate tacking with realizable control signal. In terms of the transient responses, PID scheme needs two seconds (See the top row of Fig. 10), SMC needs one second (See the top row of Fig. 13), and the remaining two approaches need slightly more than 1 seconds. Indeed, one could shorten these settling times yet in those cases the applicability of the control signals disappear. Since the results obtained so far stipulate the merits and usefulness of the devised model, instead of pointing out a specific approach as the best one, we prefer demonstrating their qualities in such an application. The selection of the most appropriate parameter values for the controllers depends on the vehicle dynamics, disturbances and

expectations of the user. The tuning process carried out is based on the trial and error search with the help of real time system being built in the UAV laboratory of TOBB ETU.

9 Concluding Remarks

Due to their low cost and versatility, UAVs find numerous application areas. This work focuses on modeling and low level control issues on a quadrotor type UAV. The vehicle model is formed then the issues of power loss during the flight are discussed and a method based on the neural network modeling is introduced to handle the time varying dynamics. It is seen that the neural models are useful in establishing the handshaking at the pwm level, which is the language in between the motors and the feedback controller. Neural network components have been developed by collecting a number of simultaneous time traces and Levenberg-Marquardt technique is utilized. The filters for transient behavior and battery modulation issues are explained. In the end, four approaches are simulated to see whether the introduced models function properly. These methods are the PID, SMC, backstepping and feedback linearization. All produced acceptably good results for some set of parameters. Although PID is simple in structure, its performance may not be adequate under conditions of severe disturbances. SMC is robust against disturbances yet it suffers from the chattering phenomenon. Backstepping and feedback linearization yield good tracking results yet they need the availability of the system nonlinearities, which is generally accepted as a drawback. The research in the UAV laboratory of TOBB Economics and Technology University is continuing toward implementing these algorithms in real time.

10 Acknowledgments

This work is supported by TÜBİTAK, grant no 107E137. The authors gratefully acknowledge the facilities of the Unmanned Aerial Vehicles Laboratory of TOBB Economics and Technology University.

References

1. T. Madani, A. Benallegue, “Control of a Quadrotor Mini-Helicopter via Full State Backstepping Technique”, IEEE Conference on Decision & Control, Page (s):1515-1520, 2006.
2. A. Tayebi, S. McGilvray, “Attitude Stabilization of a VTOL Quadrotor Aircraft” IEEE Transactions on Control Systems Technology, Vol. 14, No. 3, Page (s):562-571, 2006.

3. M. Bouchoucha, M. Tadjine, A. Tayebi, and P. Müllhaupt, "Step by Step Robust Nonlinear PI for Attitude Stabilisation of a Four-Rotor Mini-Aircraft", 16th Mediterranean Conference on Control and Automation, Page (s):1276-1283, 2008.
4. G. Hoffmann, D.G. Rajnarayan, S.L. Waslander, and D. Dostal, J.S. Jang, and C.J. Tomlin, "The Stanford Testbed of Autonomous Rotorcraft for Multi-Agent Control (STARMAC)", 23rd Digital Avionics System Conference, Vol.2, Page(s): 12.E.4 - 121-10, 2004.
5. T. Hamel, R. Mahony, R. Lozano and J. Ostrowski, "Dynamic Modeling and Configuration Stabilization for an X4-Flayer", IFAC 15th Triennial World Congress, 2002.
6. S. Bouabdallah, R. Siegwart, "Backstepping and Sliding-mode Techniques Applied to an Indoor Micro Quadrotor", IEEE International Conference on Robotics and Automation, Page(s):2247 – 2252, 2005.
7. L. Kis, G. Regula, and B. Lantos, "Design and Hardware-in-the-Loop Test of the Embedded Control System of an Indoor Quadrotor Helicopter", Intelligent Solutions in Embedded Systems, International Workshop, Page(s): 1 – 10, 2008.
8. Z. Fang, Z. Zhi, L. Jun, and W. Jian, "Feedback Linearization and Continuous Sliding Mode Control for a Quadrotor UAV", 27th Chinese Control Conference, Page(s):349-353, 2008.
9. K.H. Ang, G. Chong, and Y. Li, "PID Control System Analysis, Design and Technology" IEEE Transactions Control Systems Technology Vol. 13, No. 4, Page(s):559-576, 2005.
10. K.J. Aström, T. Hagglund, "PID Controllers:Theory,Design and Tuning", Page(s):80 - 86, ISA The Instrumentation, Systems and Automation Society, USA, 1995.
11. K.D. Young, V. Utkin, and Ü. Özgüner "A Control Engineer's Guide to Sliding Mode Control" IEEE Transactions Control Systems Technology, Vol. 7, No. 3, Page(s): 328-342, 1999.
12. V. I. Utkin, "Variable structure systems with sliding modes," IEEE Transactions Automation and Control Society, Vol. 22, Page(s): 212–222, 1977.
13. M.Ö. Efe, "Robust Low Altitude Behavior Control of a Quadrotor Rotorcraft Through Sliding Modes", Mediterranean Conference on Control and Automation, Page(s): 1-6, 2007.
14. M. Krstic, I. Kanellakopoulos, P. Kokotovic, "Nonlinear and Adaptive Control Design", Page(s): 88-99, John Wiley& Sons,Inc., USA, 1995.
15. P.V. Kokotovic, "The joy of feedback: nonlinear and adaptive" IEEE Control Systems Magazine, Vol. 12, Page(s): 7 - 17, 1992.
16. T. Madani, A. Benallegue, "Backstepping Control for a Quadrotor Helicopter" IEEE International Conference on Intelligent Robots and Systems, Page(s):3255-3260, 2006.
17. J.J.E. Slotine, W. Li, "Applied Nonlinear Control", Page(s):207-271, Prentice Hall, New Jersey 1991.
18. H. Khalil, "Nonlinear Systems", Page(s):519-570, Prentice Hall, New Jersey, 1996.
19. A. Benallegue, A. Mokhtari, L. Fridman, "Feedback Linearization and High Order Sliding Mode Observer for a Quadrotor UAV", International Workshop on Variable Structure Systems, Page(s):365-372, 2006.
20. S. Bouabdallah, R. Siegwart, "Full Control of a Quadrotor", IEEE/RSJ International Conference on Intelligent Robots and Systems, Page(s):153-158, 2007.
21. S.Bouabdallah, A. Noth, R. Siegwart, "Modelling of the (OS4) Quadrotor", Modelling Course, EPFL, 1999.
22. B. Erginer, E. Altuğ, "Modeling and PD Control of a Quadrotor VTOL Vehicle", IEEE Intelligent Vehicles Symposium, Page(s): 894-899, 2007.
23. P. Castillo, P. Albertos, P. Garcia, R. Lozano, "Stabilization of a Mini Rotorcraft with Four Rotors", IEEE Conference on Decision & Control, Vol. 25, Page(s): 45-55, 2006.

24. H. Bouadi, M. Bouchoucha and M. Tadjine, “Modelling and Stabilizing Control Laws Design Based on Sliding Mode for an UAV Type-Quadrotor”, IEEE Intelligent Vehicles Symposium, 2007.
25. M. Amir, V. Abbass “Modeling of Quadrotor Helicopter Dynamics” International Conference on Smart Manufacturing Application, Page(s):100-105, 2008.
26. G. Hoffman, D. G Rajnarayan S.L Waslander and C.J.Tomlin “The Stanford Testbed of Autonomous Rotorcraft for Multi Agent Control (STARMAC)” Digital Avionics Systems Conference page(s): 12.E.4- 121-10.2004.
27. T. Adigbli, C. Grand, J.B Mouret, S.Doncieux “Nonlinear Attitude and Position Control of a MicroQuadrotor using Sliding Mode and Backstepping Techniques” 3rd US-European Competition and Workshop on Micro Air Vehicle Systems & European Micro Air Vehicle Conference and Flight Competition, Page(s):1-9, 2007.